Ukrainian Journal of Physical Optics
ISSUE 4
2026

MACHINE LEARNING APPROACH FOR OPTICAL NON-DESTRUCTIVE NANOMETROLOGY OF NANO (MICRO) SCALE ROUGH SURFACES

C. ZENKOVA [1]*, O. ANGELSKY [1], D. IVANSKYI [1], V. TKACHUK [1], P. RYABYI [1], A. KONIAKHIN [1], YU. URSULIAK [2], S. HANSON [3]

[1] Chernivtsi National University, 2 Kotsiubynskoho Street, Chernivtsi, Ukraine, 58002
[2] Municipal Enterprise Chernivtsi Regional Clinical Cardiological Center, 230 Heroiv Maidanu, Chernivtsi, Ukraine, 58006
[3] DTU Fotonik, Department of Photonics Engineering, Frederiksborgvej 399, Building 128, 4000 Roskilde, Denmark
*Corresponding author: k.zenkova@chnu.edu.ua

Received: 15.07.2026

Abstract. A comprehensive approach for non-contact, non-destructive, and high-precision analysis of surface inhomogeneity distributions has been proposed, enabling reconstruction of the surface height distribution with coefficients of determination (R^2) ranging from 0.86 to 0.90, based on the photoluminescence intensity distribution of surface-deposited perovskite nanoparticles. Perovskite nanoparticles of about 5 nm were employed as functional markers, reproducing the surface topographic profile after deposition. A machine learning model based on graph convolutional networks (GCN) was developed to analyze and reconstruct the height distribution of surfaces with nano- and micro-inhomogeneities. The model was trained using experimental data obtained by atomic force microscopy to determine the surface height profile, together with measurements of the luminescence intensity of the deposited nanoparticles.

Keywords: perovskite nanoparticles, graph convolutional networks, height distribution, nano- and micro-inhomogeneities
UDC: 004.85:535.8, 620.179.16, 681.7
DOI: 10.3116/16091833/Ukr.J.Phys.Opt.2026.04088

1. Introduction

In the modern world, the development and advancement of a comprehensive set of methods and approaches aimed at the detection, measurement, and analysis of surface micro- and nanotopography, whose characteristics are determined by nanoscale inhomogeneities, are becoming increasingly important. Such studies enable the evaluation of geometric, structural, optical, and functional surface parameters, including roughness, height, and spatial distribution of profile inhomogeneities, correlation characteristics, as well as local defects.

At present, the primary purpose of approaches to diagnosing nanorough surfaces is to optimize material properties and functional surfaces whose characteristics are governed by nanoscale relief features, as surface nanotopography significantly influences the mechanical, optical, electrical, and adhesive properties of material surfaces.

Among the wide range of potential applications, these methods are implemented in technical fields such as mechanical engineering [1,2], micro- and nanoelectronics for the micro-/nanoanalysis of semiconductor surface structures and the investigation of photolithographic elements [3], as well as for assessing the quality of functional layers in integrated circuits, micro-electromechanical systems / nano-electromechanical systems (MEMS/NEMS) systems, and sensors with functional coatings [4]. More broadly, considering the need to study the structure of

biologically derived nanosurfaces, such methods are increasingly applied in biomedical optics, photonics, and optical engineering. In these fields, investigating the nanoroughness of optical elements, diffractive structures, metasurfaces, and waveguides enables evaluation of scattering levels, optical losses, and wavefront-formation quality.

The study and characterization of nanorough surfaces involves both contact and non-contact methods. Contact techniques, including contact profilometry and atomic force microscopy (AFM), provide high accuracy in determining the geometric parameters of surface relief at the nanoscale. However, due to the mechanical interaction between the cantilever and the surface, they may cause local damage or distortion, particularly in soft or biological materials. In addition, these methods are characterized by relatively low scanning speed and a limited investigation area.

Non-contact methods are based on the interaction of electron beams or electromagnetic radiation with the surface without physical contact. Such approaches are especially promising for investigating delicate surfaces, biologically derived nanosurfaces, and functional surfaces of optoelectronic and sensor elements, whose properties are governed by nanometer-scale relief inhomogeneities, where even minimal mechanical influence can significantly alter the morphology or functional characteristics of the object.

Among the main non-contact optical techniques, polarization-sensitive and coherent optical methods play a special role, enabling the analysis of both the phase structure and optical properties of nanorough surfaces. Several of our papers [5-12] present novel correlation-based approaches that allow investigation of the three-dimensional topology of such surfaces and extraction of statistical parameters.

In the early works reported in [10–12], two roughness measurement methodologies were proposed, based on the analysis of the phase dispersion of the boundary-object field and the transverse coherence function, along with devices implementing these approaches. The obtained measurements yield statistical field parameters evaluated within interferometric schemes with zero (infinitely extended) interference fringes. Among the developed devices [10–12], a stationary system was introduced for measuring the root-mean-square (RMS) height deviations of moderately rough surfaces in the range of 0.002 μm to 0.06 μm, as well as a portable device with a measurement range of 0.005 μm to 0.1 μm RMS deviation. The sensitivity of RMS height estimation reaches 10 Å.

Recent studies [5,6] introduce interference–correlation approaches based on joint reconstruction of amplitude and phase information from recorded speckle fields scattered by phase-inhomogeneous objects, enabling real-time prediction of surface structure with inhomogeneities on the order of the optical wavelength. Complementary works [7–9] focus on ultra-precise characterization of super-smooth surface nanotopography, achieving sensitivity beyond the transverse resolution limit defined by Abbe's criterion.

In both cases, carbon-based nanoparticles are employed as functional probes, in which surface nanorelief is retrieved by analyzing their luminescence response [7–9].

A substantial body of our papers [5-9, 16] addresses nano- and microscale optical interactions in structured media. The rationale for nanoparticle-based probing originates from systematic studies of optical fields with varying polarization and coherence states [13–18] interacting with nanostructures. Potential limitations arising from nonlinear optical effects [19], which may compromise reliable surface reconstruction, have also been investigated.

Nanoparticle-based approaches employed in [5- 9] are non-invasive and highly sensitive and can be applied to both organic and inorganic objects, enabling simultaneous measurements across the entire sample area. Nanoscale implementation of the method proposed in [7–9] requires an additional structured vortex optical beam to isolate nanoparticles and form a gradient optical trap. In this regime, nanoparticles must possess a sufficient dipole moment to ensure effective interaction with the external electric field. There is a need to find simpler, but no less effective, highly sensitive, non-invasive methods for studying nanorough surfaces.

In recent years, machine learning (ML) frameworks have increasingly been integrated into optical metrology to automate image processing, solve complex inverse scattering problems, and extract feature topographies. Machine learning has emerged as a powerful approach for predicting surface roughness because it can identify complex, nonlinear relationships between input parameters and surface characteristics. Unlike conventional analytical methods, machine learning algorithms can effectively capture hidden patterns within experimental and simulated datasets, thereby improving prediction accuracy and robustness. These approaches encompass a broad spectrum of algorithms, ranging from linear and nonlinear regression models to decision trees, random forests, support vector machines, and ensemble learning techniques. More recently, deep learning architectures, including convolutional neural networks (CNNs) [20] and graph neural networks (GNNs) [21–23], have further advanced surface characterization by enabling the analysis of complex spatial features and high-dimensional data. Among deep learning models, GNNs have attracted considerable attention because they are specifically designed to process graph-structured data. Unlike CNNs, which primarily operate on regular grid-based data, GNNs exploit both node attributes and the topological relationships between neighboring nodes, allowing them to capture complex spatial dependencies that are difficult to represent using conventional machine learning approaches. Among the different GNN architectures, Graph Convolutional Networks (GCNs) [24, 25] are the most widely adopted due to their computational efficiency and predictive performance. By aggregating information from neighboring nodes through graph convolution operations, GCNs learn informative feature representations that have proven effective in surface characterization, materials informatics, computer vision, and biological network analysis.

A comprehensive review of the application of computer technologies and artificial intelligence in surface metrology is presented in [26]. The authors emphasize that the type and quality of the data used for model training and validation are key factors determining the accuracy and generalization capability of surface roughness prediction models. Existing datasets are predominantly obtained using contact techniques, such as profilometry and AFM, or non-contact methods including optical, confocal, and laser-based imaging. Nevertheless, developing non-contact approaches capable of resolving surface topography with nanometer-scale resolution remains a significant challenge. At the same time, there is an increasing demand for accurate and generalizable artificial intelligence models capable of processing multimodal experimental data for reliable surface characterization.

The predictive performance of machine learning models is commonly evaluated using the average surface roughness parameter (Ra) [27] together with statistical validation metrics, including the root mean square error (RMSE) and the coefficient of determination (R^2) [28]. While RMSE quantifies the average prediction error, the coefficient of determination measures the proportion of variance in the target variable explained by the predictive model, making it one of the most informative metrics for assessing regression performance.

A recent study [28] investigated the prediction of surface roughness for synthetically generated surfaces with an average roughness of approximately 200–300 nm using ensemble machine learning algorithms. Model performance was evaluated using RMSE and R^2, enabling the identification of the most accurate prediction algorithm. However, the proposed framework was developed for statistically generated surface datasets and focused on predicting scalar roughness parameters rather than reconstructing the complete nanoscale surface topography from experimental imaging data.

The integration of AFM with machine learning has also been successfully applied to the characterization of layer-by-layer (LbL) polyelectrolyte films [29]. In this approach, AFM topographical maps served as the reference data for training predictive models, demonstrating that machine learning can significantly improve surface morphology analysis. However, despite the advantages of combining AFM with artificial intelligence, AFM remains an inherently contact-based technique that requires direct mechanical interaction between the probe and the sample surface. Such interaction may lead to deformation or damage of fragile nanostructures, thereby limiting its applicability to sensitive materials. These limitations motivate the development of non-contact imaging approaches combined with advanced deep learning algorithms capable of reconstructing nanoscale surface topography without physically affecting the specimen.

In this regard, the paper proposes using specially synthesized luminescent perovskite nanoparticles ($CsPbBr_3$), stabilized in ethylbenzene, with an average size of about 5 nm [30], which were uniformly applied to the studied surfaces with nano- and micro-inhomogeneities so that their spatial distribution repeated the relief. The synthesized nanoparticles retained their luminescent properties for up to 30 days [30]. Due to their nanometric dimensions, after application, a thin luminescent layer was formed, the thickness of which was commensurate with the size of the nanoparticles. The luminescence intensity was recorded by raster scanning the sample with a step of 0.35 μm in the horizontal and vertical directions. To increase the spatial density of the measurements, the initial scanning point was sequentially shifted by 50 nm along each coordinate axis. During the experiment, the relative position of the sample, the excitation source, and the luminescence recording system remained unchanged, which ensured stable excitation and radiation collection conditions. Under such conditions, the change in luminescence intensity is determined primarily by the location of the emitting centers that fall into the excitation and recording zone [7]. Since the deposited layer of nanoparticles conformally repeats the nanorelief of the surface, local changes in height change the spatial location of the luminescent centers relative to the excitation region and the radiation collection region. This, in turn, leads to a change in the recorded luminescence intensity, which is measured by a Raman spectrometer. As a result, the recorded luminescence intensity is a monotonic function of the local surface height. Thus, the distribution of luminescence intensity [7] contains physically based information about the local topography of the surface and can be used as an input data set for the reconstruction of its spatial relief.

Thus, in this work, a method for non-destructive reconstruction of surface nanotopography involving luminescent perovskite nanoparticles is proposed, which is based on the use of GCN. The model learns to establish a correspondence between the spatial distribution of luminescence intensity and the absolute values of the surface height obtained from AFM, which are used as reference data. By dynamically constructing *k*-nearest neighbor (*k*-NN) graph topologies and aggregating high-dimensional topological node features, the model effectively captures non-linear spatial dependencies, offering a robust computational tool for non-destructive nanosurface topography reconstruction.

2. Measurement methodology and validation

The proposed comprehensive approach to the diagnosis and investigation of surface nanotopography of rough surfaces involves a sequence of experimental and computational steps. The first stage consists of measuring the distribution of surface inhomogeneities on surfaces with nano- and microtopography using AFM; the resulting data are used as a reference dataset to train the machine learning algorithm and to validate the reconstructed surface height parameters.

The surfaces selected for the study were those with roughness parameters in the vicinity of Ra: 2.896 nm, Rq: 3.737 nm, Rsk: 1.263 Rku: 28.108 (smooth surfaces) and with roughness parameters in the vicinity of Ra: 298.994 nm, Rq: 402.785 nm, Rsk: 0.038, Rku: 1.514 (matte surfaces). The samples size were about 45x45 μm^2. 120 samples with different surface types were analyzed.

In the course of the work, an experimental method of reproducing the surface relief was tested, which is based on the use of perovskite nanoparticles (perovskite nanomaterials) ($CsPbBr_3$), with a thickness of about 5 nm, which are applied to the surfaces under study using a 1 μl pipette dispenser. The particles are characterized by absorption at an excitation wavelength of 405 nm; the maximum of luminescence corresponds to a wavelength of 531 nm. The nanoparticle synthesis methodology is described in detail in [30]. Among various classes of perovskite nanomaterials, $CsPbBr_3$ represents a distinct group of fully inorganic nanoscale structures combining enhanced stability, high photoluminescence quantum yield, narrow emission linewidth, tunable bandgap, and facile synthesis. The nanoparticles are stabilized with polystyrene, which enables controlled spatial distribution on the surface and efficient photoluminescence detection. Upon deposition onto the surfaces, the nanoparticles are statistically distributed with equal probability across local height extrema, effectively conforming to the nanoscale surface relief.

Luminescence intensity measurements were performed stepwise over the entire sample area at the excitation wavelength using a Renishaw inVia Raman spectrometer (GRAMS/32 software). For each surface, 130×130 intensity values were obtained.

The system was operated in photoluminescence mode by applying a spectral filter that isolated the emission band corresponding to the luminescence excitation. The Raman spectrometer used a dry microscope objective lens, Leica Germany 566027 50×/0.75 N Plan; excitation was performed with a Cobolt 08-NLD 405 nm laser at 30 mW.

Transverse (x,y) reconstruction, implemented in this work, relies on nanoparticle separation through deconvolution of the measured transverse intensity distribution in cases of particle overlap using the point spread function (PSF). The PSF describes the imaging response of a single fluorescent point source in the system and was estimated theoretically and refined through optimization of luminescence intensity values. The optimization procedure involved iterative adjustment of the PSF width, focal position, and blur parameters during blind deconvolution until the reconstructed image achieved the highest structural similarity and minimum reconstruction error with respect to the experimentally acquired fluorescence images. Image deconvolution was performed using the blind deconvolution function (*deconvblind*) implemented in MATLAB. This function is based on the iterative Lucy–Richardson maximum-likelihood algorithm, which simultaneously estimates both the latent image and PSF. During each iteration, the algorithm updates the image and

the PSF to maximize the likelihood of the observed data under the assumption of Poisson-distributed noise, making it particularly suitable for further processing.

To convert luminescence intensity distributions into quantitative surface nanorelief height maps, a GCN was developed and validated. The trained model reconstructs the surface morphology by predicting the surface height profile along the longitudinal $z(x)$ direction. The proposed GCN was trained using a dataset comprising AFM surface height maps and the corresponding luminescence intensity measurements acquired at identical spatial locations before and after the deposition of perovskite nanoparticles. The measured intensity serves as a set of spatially resolved input features that encode information about the underlying surface morphology. To represent the complex, irregular geometry of nanostructured surfaces without introducing interpolation artifacts associated with regular grids, the experimental measurements are directly mapped onto an adaptive graph structure, $\mathcal{G}=(\mathcal{V},\mathcal{E})$, where the vertices correspond to measurement points and the edges describe their local spatial relationships.

Each experimental measurement point within a sample is defined as a graph node $v_i \in \mathcal{V}$, located at spatial coordinates $\mathbf{p}_i = (X_{um}, Y_{um}) \in \mathbb{R}^2$. The primary input feature for node v_i is the locally normalized luminescence intensity $I_{norm,i}$. To ensure robustness against baseline intensity shifts across independent experimental measurements, local dynamic Min-Max scaling is executed per sample: $I_{norm,i} = \dfrac{I_i - \min(\mathbf{I})}{\max(\mathbf{I}) - \min(\mathbf{I}) + 10^{-6}}$. Here $I_{\mathrm{norm},i}$ - normalized luminescence intensity value for the i-th measurement point (graph node), a scalar value of which is in the range $[0,1]$, I_i - initial (measured) photoluminescence intensity at the i-th measurement location, $\mathbf{I}$ - vector/array of all intensity values for a specific experimental sample, $\min(\mathbf{I})$ - minimum intensity value among all points within a single experimental sample, $\max(\mathbf{I})$ - maximum intensity value among all points within a single experimental sample, 10^{-6} - small regularization constant (ϵ) added to the denominator to prevent division by zero in case of identical intensity values.

Spatial connectivity is established dynamically using a k-Nearest Neighbors (k-NN) algorithm in the spatial coordinate domain ($k = 8$), creating undirected graph edges $e_{ij} \in \mathcal{E}$ between neighboring fluorescent markers. The relative spatial distance between adjacent nodes is embedded as a continuous edge weight w_{ij} using an exponential decay kernel: $w_{ij} = \exp\left(-\dfrac{\| \mathbf{p}_i - \mathbf{p}_j \|_2}{\max(\| \mathbf{p}_k - \mathbf{p}_l \|_2) + 10^{-6}} \right)$, where w_{ij} - weight of the direct (adjacent) edge $e_{ij} \in \mathcal{E}$ between nodes i and j, representing spatial proximity, $\mathbf{p}_i, \mathbf{p}_j$ - 2D spatial coordinate vectors of the i-th and j-th points, respectively: $\mathbf{p}_i = (X_i, Y_i) \in \mathbb{R}^2$, $\| \mathbf{p}_i - \mathbf{p}_j \|_2$ - Euclidean distance (2-norm) in physical coordinates (μm) between points i and j, $\max(\| \mathbf{p}_k - \mathbf{p}_l \|_2)$ - maximum Euclidean distance between any two connected points k and l within the sample (used for distance normalization), $\exp(\ldots)$ - exponential decay function that decreases edge weight as the physical distance between nodes increases.

GCNs are particularly well suited for capturing such non-Euclidean spatial dependencies in surface morphology. The network architecture, implemented in PyTorch Geometric, is presented in Fig. 1.

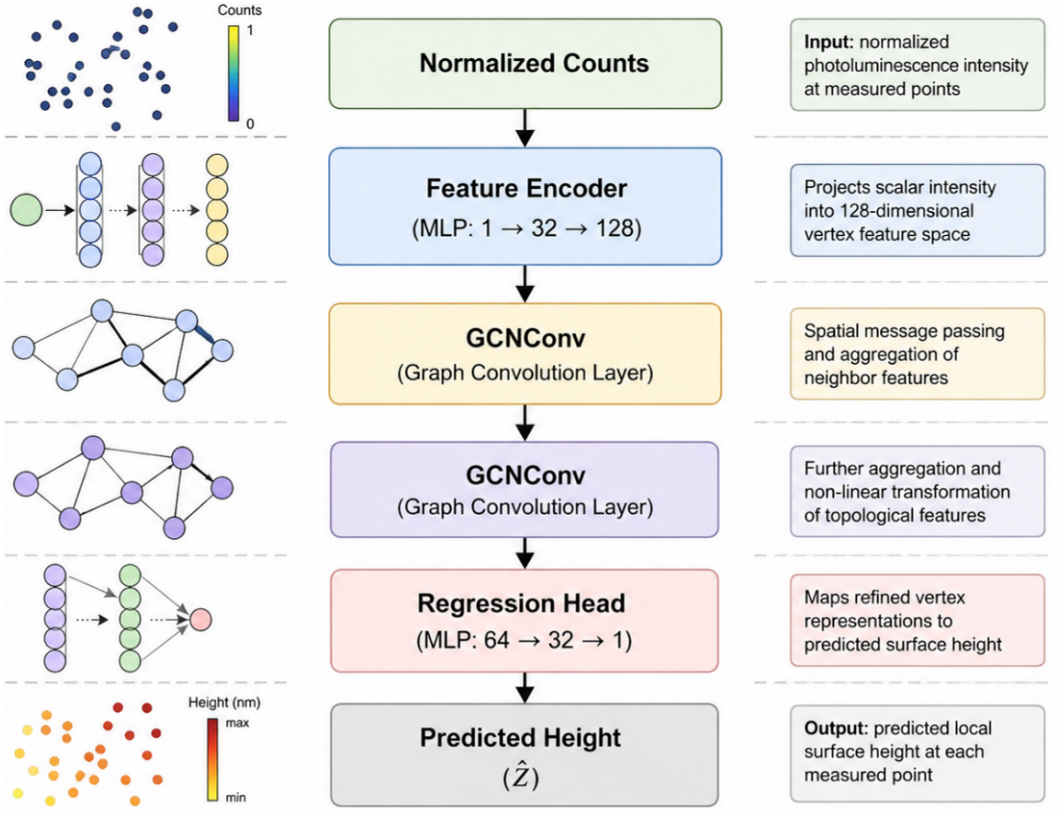

Fig. 1. Model architecture diagram.

Feature Encoding Layer. A Multi-Layer Perceptron (Linear $1 \to 32 \to 128$ with ReLU activations) that projects the scalar normalized intensity feature into a high-dimensional node representation space $\mathbf{h}_i^{(0)} \in \mathbb{R}^{128}$.

Graph Convolutional Backbone. Two sequential Graph Convolutional (GCNConv) layers. Spatial message passing aggregates non-linear topological feature representations from adjacent nodes weighted by w_{ij}: $\mathbf{h}_i^{(l+1)} = \mathrm{ReLU}\left(\mathbf{W}^{(l)} \sum_{j \in \mathcal{N}(i)} \frac{w_{ij}}{\sqrt{\hat{d}_i \hat{d}_j}} \mathbf{h}_j^{(l)}\right)$, where $\mathbf{h}_i^{(l)}$-hidden feature representation vector of the i-th node at layer l, at input ($l = 0$): $\mathbf{h}_i^{(0)} \in \mathbb{R}^{128}$ after passing through the Feature Encoder, $\mathbf{h}_i^{(l+1)}$ - updated feature vector of the i-th node after passing through the $(l+1)$-th convolution layer, $\mathbf{W}^{(l)}$ - trainable weight matrix of the l-th graph convolutional layer, $\mathcal{N}(i)$ – set of adjacent neighbors of the i-th node, determined by the k-Nearest Neighbors algorithm (k-NN with $k = 8$), w_{ij} – calculated edge weight between nodes i and j, $\hat{d}_i, \hat{d}_j$ –weighted degree of nodes i and j, respectively. Computed as the sum of adjacent edge weights: $\hat{d}_i = \sum_{j \in \mathcal{N}(i)} w_{ij}$, $\frac{w_{ij}}{\sqrt{\hat{d}_i \hat{d}_j}}$ - normalized connectivity weight used to balance contribu tions from nodes with varying local cluster densities (symmetric normalization). ReLU –non-linear activation function $\mathrm{ReLU}(z) = \max(0, z)$.

Regression Head. A fully connected prediction block (Linear $64 \to 32 \to 1$) that maps the refined graph node embeddings directly to the target local surface height, measured by AFM, $Z_{AFM} \in \mathbb{R}^1$. To guarantee independent model validation and completely prevent data leakage, the complete dataset of graph instances was partitioned into a training set (80%) and an independent held-out validation set (20%) prior to neural network optimization.

The neural network was optimized using the Adam algorithm with an initial learning rate of $\eta = 10^{-3}$ and an L_2 weight decay regularization parameter of $\lambda = 10^{-4}$ to prevent overfitting to local cluster densities. Optimization was performed over 100 training epochs using a batch size of eight graph instances. The network parameters were optimized by minimizing the mean squared error (MSE) loss function defined as $\mathcal{L}_{MSE} = \frac{1}{N}\sum_{i=1}^{N}\left(\hat{Z}_i - Z_{AFM,i}\right)^2$, where $\hat{Z}_i$ – is the surface height predicted by the GCN model, and N – is the number of sampling points (graph nodes). During validation cycles, the model was executed strictly in evaluation mode (model.eval()) with gradient computation disabled (torch.no_grad()) on the isolated validation graphs.

Model performance was evaluated on an independent validation dataset using the coefficient of determination ($R^2 = 1 - \sum \frac{\left(\hat{Z}_i - Z_{AFM,i}\right)^2}{\left(\bar{Z}_i - Z_{AFM,i}\right)^2}$) ranging from 0.86 to 0.90 ($\bar{Z}_i$ -sample mean) and a Root Mean Squared Error ($\mathrm{RMSE} = \sqrt{\sum_{i=1}^{N}\left[\left(\hat{Z}_i - Z_{AFM,i}\right)^2 / N\right]}$) in the range of 0.09–0.12 nm, evaluated alongside the Mean Absolute Error ($\mathrm{MAE} = \frac{1}{N_{val}}\sum_{i=1}^{N_{val}}\left|\hat{Z}_i - Z_{AFM,i}\right|$,) which varies within 0.06-0.09 nm. These performance metrics were consistent with AFM-based height measurement precision on nanoparticle-free baseline surfaces. Metrics computed on the held-out validation set served exclusively for monitoring model generalization capabilities and hyperparameter tuning, ensuring that validation data never participated in gradient updates or parameter weight optimization.

3. Results and discussion

Two types of surfaces were investigated: an opaque glass plate with a polished surface and an opaque glass plate with a rough surface. All measurements were performed in reflected radiation. AFM was used to construct the dataset for neural network training and validation. A database of surface height profiles was compiled for samples both without and with deposited nanoparticles.

The smooth surface without nanoparticles was characterized by roughness parameters of $R_a \backsim 2.896$ nm and $R_q \backsim 3.737$ nm, whereas the rough surface without nanoparticles exhibited $R_a \backsim 298.868$ nm and $R_q \backsim 360.726$ nm, respectively. Surface profiles were obtained using AFM (Fig. 2), and the autocorrelation length was evaluated as the lateral distance at which the autocorrelation function decays to 0.2. From the computed autocorrelation distributions (Fig. 2b, c), the autocorrelation length was estimated as R_{al} = 440 nm for the smooth surface and R_{al} = 3.5 μm for the rough surface. The resulting dataset constituted the initial training set for the neural network model.

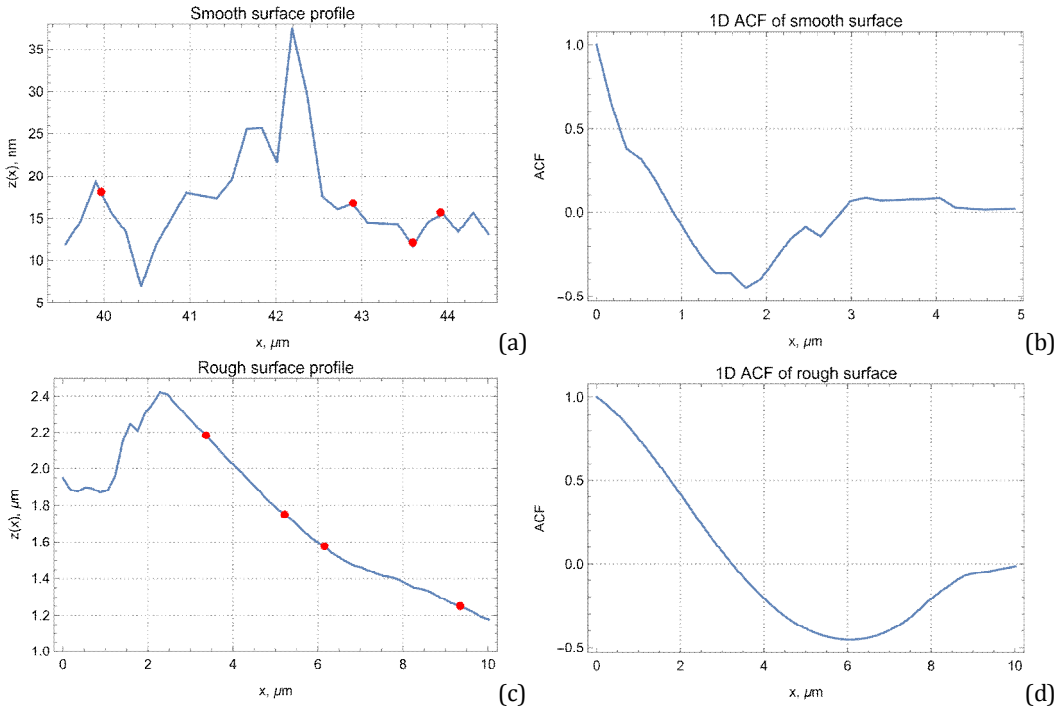

Fig. 2. Surface profiles of the polished (a) and rough (c) surfaces along the x-direction (y=0) relative to the baseline (z = 0), obtained by AFM, with indication of particle position, marked in red. Autocorrelation functions for the polished (b) and rough (d) surfaces, respectively.

The next step involved deposition of nanoparticles onto the investigated surfaces. The surface height profiles were measured using AFM, enabling identification of nanoparticle localization points and the construction of an additional dataset for neural network training.

Imaging of samples with deposited nanoparticles, with determination of spatial coordinates, for the purpose of further recording of photoluminescence by a Raman spectrometer (Fig. 3a), was performed using a MICROmed Evolution LUM LS-8530 fluorescence microscope equipped with a WF16×/13 eyepiece, an Infiniti Plan 40×/0.65 (S) objective, and a 100 W/DC mercury lamp with a dual-fluorescence filter system. Fluorescence microscopy images were processed in MATLAB using a multistage image analysis workflow. The acquired color images were first converted to 8-bit grayscale (256 intensity levels), followed by region-of-interest selection, image binarization, noise suppression, particle detection and segmentation, and centroid extraction. Accordingly, the algorithm searches for a marker point (particles) in red in the figure (Fig. 3), and the intensity value is identified with the grayscale value at this point (in yellow) (Fig. 3b,d). Accurate luminescence intensity spectra in the spatial coordinates selected by the microscope were measured using a Raman spectrometer. The centroid coordinates and the corresponding luminescence intensities were subsequently used to construct the graph nodes for the GCN and to analyze the spatial distribution of the luminescent nanoparticles.

Based on the photoluminescence intensity distributions of spatially distributed nanoparticles at selected measurement points, correlation and regression analyses were performed to establish the relationship between emission intensity and surface height (Fig. 4).

The results are shown for the rough (Fig. 4a) and smooth (Fig. 4 b) surfaces. The blue line is a simulated linear regression model predicting the relationship between luminescence intensity and profile height relative to the measured surface height values (Fig. 2a, c) at marker red points (the same surface points without and with particles), by atomic force microscopy.

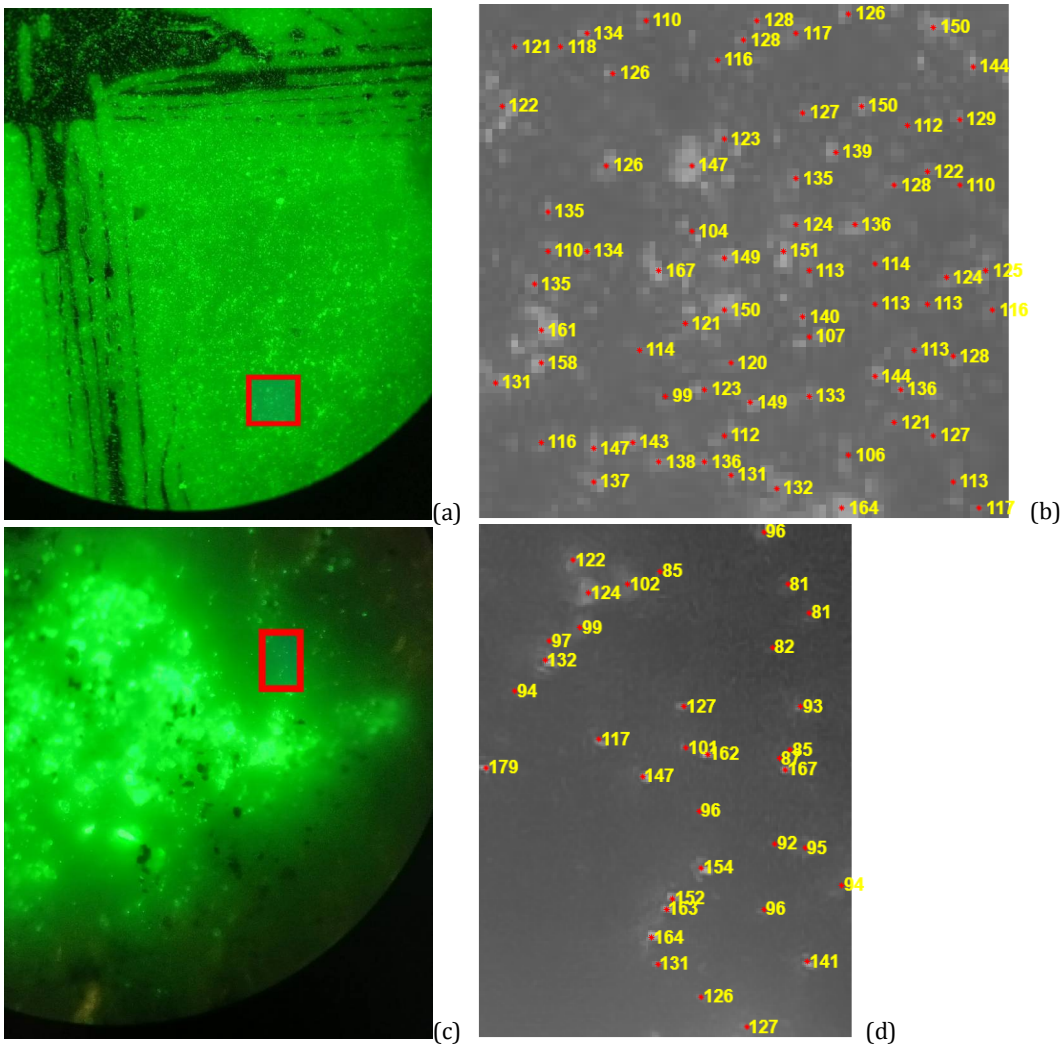

Fig. 3. Example of a smooth (a) and rough (c) surfaces with nanoparticles in a fluorescence microscope, the blue square indicates the area that is magnified for smooth (b) and rough (d) surfaces, correspondingly, with the positions of the nanoparticles (red points) and luminescence intensity (yellow numbers). The intensity value is identified with the grayscale value at that point.

The quality (goodness) of the linear regression model was assessed the coefficient of determination $R^2 = 0.48$ (smooth surface) and $R^2 = 0.50$ (rough surface), respectively, and the regression error was measured by the root mean squared error (RMSE) (the standard error of the regression (SER) or standard error of the estimate (SE)): $RMSE = 0.197$ nm (smooth surface) and $RMSE = 0.159$ nm (rough surface). The linear regression model obtained from the experimental data analysis was used during the feature engineering stage to generate the initial node features for the GCN. As already noted, the values of the height parameters of surfaces without applied nanoparticles, obtained using AFM, were used as reference data for the formation and training of the machine learning algorithm.

An example (Fig. 5) of reproducing the height distribution of smooth (rough) surfaces, obtained using AFM and the corresponding GCN prediction in the form of a height map, is shown in Fig. 5b, d. For comparison, Fig. 5a,c shows the height map of the original smooth (rough) surface, corresponding to AFM measurements.

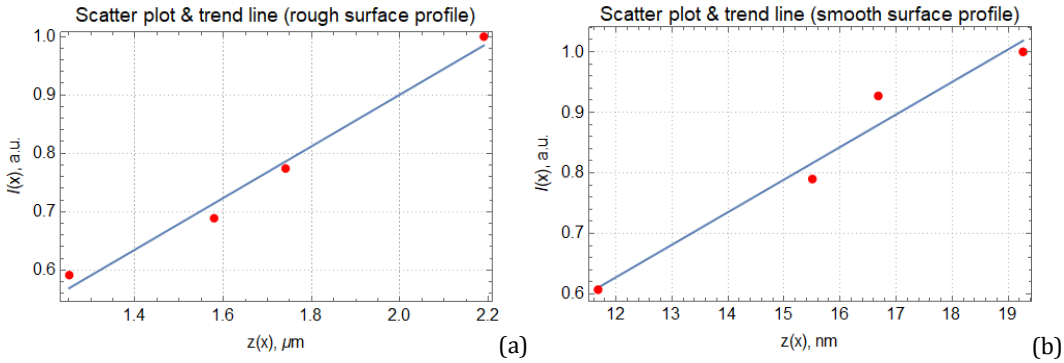

Fig. 4. Linear model of the relationship between the luminescence intensity in arbitrary units and the profile height in the case of (a) rough and (b) smooth surfaces. Here, the red dots indicate the experimentally measured intensity values for marker points on surfaces of different heights. The blue lines specify the model distribution of the intensity.

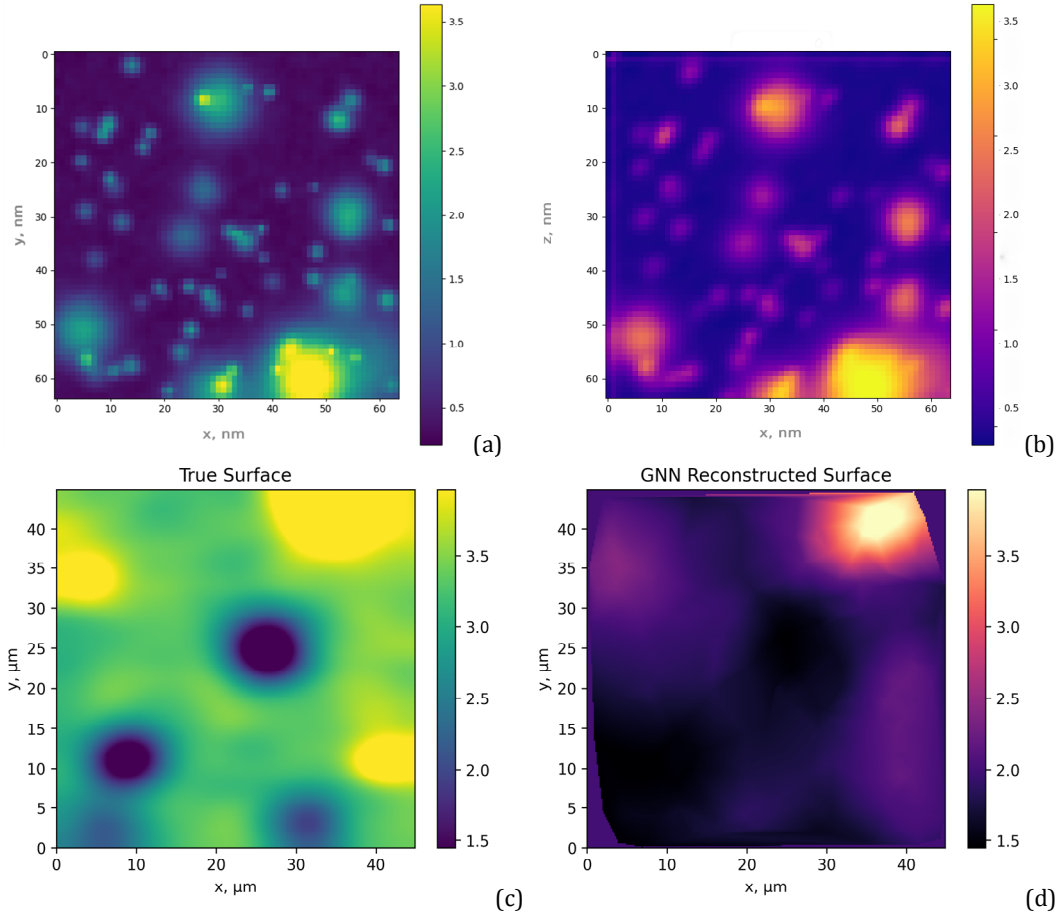

Fig. 5. Height map of the original smooth (a) and rough (c) surfaces in the nanometer (micro) range obtained by AFM, and the corresponding surface reconstruction predicted by the GCN model (b,d).

Visualization of the reconstruction results (Fig. 5) shows that the proposed GCN successfully reproduces the main spatial characteristics of the surface nanorelief. The reconstructed height maps are in good agreement with the reference AFM data, which is confirmed by the high values of the coefficient of determination R^2 (0.86–0.9) and low values of the root mean square error $RMSE$ (0.09–0.12) nm.

For comparison, a linear regression model was used, based on experimental data, to describe the direct relationship between the luminescence intensity of perovskite nanoparticles and the local height of the surface with a layer of nanoparticles applied, measured by atomic force microscopy. Since such a model takes into account only the linear relationship between the specified parameters and does not describe their spatial relationships, it demonstrated significantly lower prediction accuracy than the proposed GCN. The GCN increased the coefficient of determination by approximately 0.40 compared with the linear regression model. The result indicates GCN's ability to effectively account for complex nonlinear spatial relationships between the photoluminescence intensity distribution and surface topography that are not available to classical linear models.

In general, the results demonstrate that the developed machine-learning algorithm can reconstruct the surface height distribution with coefficients of determination R^2, ranging from 0.86 to 0.90, based on the photoluminescence intensity distribution of surface-deposited perovskite nanoparticles.

4. Conclusions

The paper presents the results of a comprehensive approach to reproducing the height distribution of surfaces with nano (micro) inhomogeneities, where the machine learning model generated using GCN played a crucial role; the training of which was carried out on the basis of measurement data of both the height distribution using AFM and the measurement of the luminescence intensity of nanoparticles. It was proposed to use perovskite nanoparticles, about 5 nm in size, which, when applied to the surface, replicated the height distribution of surface inhomogeneities. A key aspect of the proposed approach is the implementation of non-contact high-precision surface analysis, which increased the coefficient of determination by approximately 0.40 compared with the linear regression model.

Funding and acknowledgments. This work was supported by the National Research Foundation of Ukraine (NRFU), project 2025.07/0069 “Recent applications of structured optical fields in polarization-interference methods for solving problems in telecommunications and biomedicine”. The authors are grateful to Dr.Yurij Khalavka (vice-rector of Chernivtsi National University, Ukraine) and his colleagues from the Department of Chemistry and Food Expertise (Chernivtsi National University, Ukraine) for fruitful discussion regarding the evaluation of the optical properties of perovskite nanoparticles and for assistance in organizing the experimental part of the research.

Disclosures. The authors declare no conflicts of interest.

Author’s contributions. All authors contributed substantially to the conception, design, and completion of this work: C.Z. - research concept and design; data analysis and interpretation; writing the paper; V.T. - experimental data collection; D.I. - experimental data processing; P.R., A.K. - GCN model development, code writing; O.A., Yu.U., S.H.- critical revision and final approval of the paper.

References

1. Mellor, L. (2025). Tribology in Mechanical Engineering: Navigating the Science of Friction Wear, and Lubrication. *J Appl Mech Eng*, 14, 530.
2. Ahmadi, A. (2025). Study in Tribology Science and its Importance in Mechanical Engineering. *International Journal for Multidisciplinary Research (IJFMR)*.

3. Dai, Z.X., Ono, T., Dai, C.L. (2026). Editorial for the Special Issue on MEMS/NEMS Devices and Applications, *3rd Edition. Micromachines (Basel),* 17(2), 205.
4. Daniyal, W. M. E. M. M., Fen, Y.W., Abdullah, J., Sadrolhosseini, A.R., Mahdi, M.A. (2021). Design and Optimization of Surface Plasmon Resonance Spectroscopy for Optical Constant Characterization and Potential Sensing Application: Theoretical and Experimental Approaches. *Photonics*, 8, 361.
5. Angelsky, O. V., Zenkova, C. Yu., Hanson, S. G., Ivansky, D.I., Tkachuk, V.M., and Jun Zheng (2021). Random object optical field diagnostics by using carbon nanoparticles, *Optics Express*, 29(2), 916-928.
6. Angelsky, O. V., Zenkova, C. Yu., Ivansky, D. I., Tkachuk, V. M., Jun Zheng. (2021) Carbon nanoparticles for study complex optical fields, *Journal of Optoelectronics and Advanced Materials*, 23(5-6), 2021.
7. Angelsky, O. V., Bekshaev, A. Y., Zenkova, C. Yu., Ivansky, D. I., Zheng, J., Tkachuk, V. M. (2022). Fluorescence Record Diagnostics of 3D Rough-Surface Landscapes With Nano-Scale Inhomogeneities, *Front. Phys*,
8. Zenkova, C. Yu., Ivansky, D. I., Tkachuk, V. M., and Jun Zheng. (2022). Structured Light in Applications Related to the Reconstruction of Three-Dimensional Landscape of Nanorough Surfaces, *Optical Memory and Neural Networks*, 31(1), 22–35.
9. Angelsky, O., Bekshaev, A., Zenkova, C., Ivanskyi, D., Maksymyak, P., Kryvetsky, V., Zhebo Chen. (2023). Application of the Luminescent Carbon Nanoparticles for Optical Diagnostics of Structure-Inhomogeneous Objects at the Micro- and Nanoscales, *Optical Memory and Neural Networks*, 32(4), 258–274.
10. Angelsky, O., Maksymyak, P., Zenkova, C., Ushenko, O., & Zheng, J. (2021). New Trends of Optical Measurements. In (Ed.), *Applied Aspects of Modern Metrology, IntechOpen*.
11. Angelsky, O.V., Maksymyak, P.P., Zenkova, C.Yu., Hanson, S.G., Jun Zheng. (2020). Current Trends in Development of Optical Metrology. *Optical Memory & Neural Networks (Information Optics)*, 29(4), 269-292.
12. Angelsky, O.V., Bekshaev, A.Y., Maksimyak, P.P, Mokhun, I.I., Zenkova, C.Y., Gotsulskiy, V.Y, Ivanskyi, D.I., Zheng, J. (2024). Correlation and singular optics for diagnostics of structured light and condensed matter: time-stationary and spatio-temporal approaches. *Front. Phys.* 12, 1383256.
13. Zenkova, C. Yu., Gorsky, M. P., Ryabiy, P. A., Angelskaya, A O. (2016). Additional approaches to solving the phase problem in optics. *Applied Optics* , 55(12), B78–B84.
14. Zenkova, C. Yu. (2014). Interconnection of polarization properties and coherence of optical fields. *Applied Optics*, 10, B43–B52.
15. Zenkova, C. Yu., Yermolenko, S. B., Angelskaya, A. O., Soltys, I. V. (2011). The polarization peculiarities of the correlation (Intrinsic Coherence) of optical fields. *Optical Memory and Neural Networks (Information Optics)*, 20(4), 247–254.
16. Zenkova, C. Yu., Gorsky, M. P., Soltys, I. V., Angelsky, P. O. (2012). Influence of the Brownian movement on the motion of nano and micro-particles in the inhomogeneous optical field. *Opto-Electronics Review*, 20(3), 247–254.
17. Angelsky, O. V., Bekshaev, A. Y., Zenkova, C. Yu., Ivansky, D. I., Zheng, J. (2022). Correlation Optics, Coherence and Optical Singularities: Basic Concepts and Practical Applications, *Front. Phys*.
18. Angelsky, O. V., Bekshaev, A. Y., Vasnetsov, M. V., Zenkova, C. Yu., Maksimyak, P. P., Zheng J. (2022). Optical phase singularities: Physical nature, manifestations and applications, *Front. Phys*.
19. Nitsowich, B. M., Zenkova, C. Yu. (1995). Theory of optical bistability in the region of exciton resonances, *Optical Engineering*, 34(4), 1072–1078.
20. Reza, M.H., Sibly, M.N.B., Rabbani, S.G. et al. (2026). A comprehensive review of convolutional neural networks: foundations, enhancements and applications, *Neural Comput & Applic*, 38, 56.
21. Zhou, J., Cui, G., Hu, Sh., Zhang, Zh., Yang, Ch., Liu, Zh., Wang ,L., Li, Ch., Sun, M. (2020). Graph neural networks: A review of methods and applications, *AI Open*, 1, 57-81.
22. Sharma, A. and Sharma, A. (2025). Graph Neural Network (GNN) and its Application: A State-of-the-Art Survey, *2025 IEEE International Conference on Big Data (BigData)*, Macau, China, 6763-6772.
23. Hussaine, S.M. (2025). Graph Neural Networks (GNNs) Applications. In: Chelliah, P.R., Whig, P., Nagarajan, S., Sakthivel, U., Yathiraju, N. (eds) Graph Neural Networks: Essentials and Use Cases. Springer, Cham.
24. Zhang, S, Tong, H, Xu, J, Maciejewski, R.(2019). Graph convolutional networks: a comprehensive review. *Comput Soc Netw*., 6(1), 11.
25. Wei, Yu., Wu, D. (2023). Model-based real-time prediction of surface roughness in fused deposition modeling with graph convolutional network-based error correction, *Journal of Manufacturing Systems*,71, 286-297.
26. Sourish, Gh., Knoblauch, R., Mansori, M.El., Corleto, Ci. (2024). Towards AI driven surface roughness evaluation in manufacturing: a prospective study, *Journal of Intelligent Manufacturing*, 36 (7), 4519-4548.
27. Steege, T., Bernard, G., Darm, P., Kunze, T., Lasagni, A.F. (2023). Prediction of Surface Roughness in Functional Laser Surface Texturing Utilizing Machine Learning, *Photonics*, 10, 361.

28. Sharma, A., Saini, R. S., Kaushik, A., Okshah, A., Kuruniyan, M.S., Gurumurthy, V., Vyas, R.,. Binduhayyim, R.I.H., Heboyan, A. (2025). Machine learning based approach for surface roughness prediction in precision dental prototyping, *Scientific Reports*, 15(1).
29. Aglikov, A.S., Aliev, T.A., Zhukov, M.V., Nikitina, A.A., Smirnov, E., Kozodaev, D.A., Nosonovsky, M.I., Skorb, E.V. (2023). Topological Data Analysis of Nanoscale Roughness of Layer-by-Layer Polyelectrolyte Samples Using Machine Learning, *ACS Appl. Electron. Mater*.,5 (12), 6955–6963.
30. Pylypko, V. G., Ivanitska, V. G., Khalavka, Y. B., and Krupko, O. V. (2025). Effect of oleylamine content on the optical properties of $CsPbBr_3$ nanoparticles synthesized in the presence of various antisolvents*, Proc. SPIE*, 13813, 138132Z.

Zenkova, C., Angelsky, O., Ivanskyi, D., Tkachuk, V., Ryabyi, P., Koniakhin, A., Ursuliak, Yu., Hanson, S. (2026). Machine Learning Approach for Optical Non-Destructive Nanometrology of Nano (Micro) Scale Rough Surfaces. *Ukrainian Journal of Physical Optics*, *27*(4), 04088 – 04101. doi: 0.3116/16091833/Ukr.J.Phys.Opt.2026.04088

Анотація. *Запропоновано комплексний підхід до безконтактного, неруйнівного та високоточного аналізу розподілу неоднорідностей поверхні, який дозволяє прогнозувати реконструйований розподіл висоти поверхні з коефіцієнтами детермінації R^2 у діапазоні від 0,86 до 0,90 на основі розподілу інтенсивності фотолюмінесценції поверхнево осаджених перовськітних наночастинок. Наночастинки перовскіту розміром приблизно 5 нм використовувалися як функціональні маркери, що відтворюють топографічний профіль поверхні після осадження. Для аналізу та реконструкції розподілу висоти поверхонь з нано- та мікронеоднорідностями було розроблено модель машинного навчання на основі графових згорткових мереж (GCN). Модель була навчена на основі експериментальних даних, отриманих за допомогою атомно-силової мікроскопії, для визначення профілю висоти поверхні, а також вимірювань інтенсивності люмінесценції осаджених наночастинок.*

Ключові слова: *наночастинки перовскіту, графові згорткові мережі, розподіл висоти, нано- та мікронеоднорідності*